Effects of Free Carriers on the Optical Properties of Doped CdO for Full-Spectrum Photovoltaics

Chao Ping Liu,[1] Yishu Foo,[1] M. Kamruzzaman,[1] Chun Yuen Ho,[1] J. A. Zapien,[1] Wei Zhu,[2,3] Y. J. Li,[2,4] Wladek Walukiewicz,[2] and Kin Man Yu[1*]

[1]*Department of Physics and Materials Science, City University of Hong Kong, 83 Tat Chee Avenue, Kowloon, Hong Kong*

[2]*Materials Sciences Division, Lawrence Berkeley National Laboratory, 1 Cyclotron Road, Berkeley, California 94720, USA*

[3]*Department of Physics and Center for Physical Experiments, University of Science and Technology of China, Hefei, Anhui 230026, Peoples' Republic of China*

[4]*State Key Laboratory of Luminescent Materials and Devices, and Institute of Optical Communication Materials, South China University of Technology, Guangzhou 510641, China*

(Received 13 September 2016; revised manuscript received 29 November 2016; published 28 December 2016)

CdO-based transparent-conducting oxide thin films have great potential applications in optoelectronic devices due their high mobility, low resistivity, and high transparency over a wide spectral range. In this paper, we report the results of a comprehensive study of optical properties of CdO thin films doped with different donors (In, Ga, V, Ti) with a carrier concentration in the range of 10^{20} to $>10^{21}/\mathrm{cm}^3$. Variable angle spectroscopic ellipsometry (SE) studies reveal that the complex dielectric function of CdO thin films drastically depends on the carrier concentration. Specifically, with increasing carrier concentration, (1) the net effect of Burstein-Moss shift and band-gap renormalization gives rise to an increase in the optical band gap from 2.6 to 3.2 eV; (2) the free-carrier absorption coefficient at a wavelength of 1200 nm increases from 10^2 to 1×10^4 cm^{-1}; (3) the refractive index decreases from 2.4 to 2.05 at 600 nm; (4) the high-frequency dielectric constant reduces from 5.5 to 4.8. The SE results are analyzed with results from Hall measurements to obtain information on the electron effective mass and optical mobility of CdO thin films. The significantly higher effective mass of V- and Ti-doped CdO thin film is attributed to the modification of the conduction band due to an anticrossing interaction between the localized *d* levels of V and Ti atoms and the CdO conduction-band extended states. The effective mass of In- and Ga-doped CdO increases with the electron concentration, consistent with the prediction from the nonparabolic conduction-band model. We also find that the optical mobility μ_{opt} is close to the Hall mobility μ_{Hall} when the $\mu_{\mathrm{Hall}} < 60$ $\mathrm{cm}^2/\mathrm{V\,s}$, while $\mu_{\mathrm{opt}} < \mu_{\mathrm{Hall}}$ for materials with higher μ_{Hall}.

DOI: 10.1103/PhysRevApplied.6.064018

I. INTRODUCTION

Transparent conductors are an essential component in many electronic devices including portable electronics, flat-panel displays, low-*e* windows, and solar cells [1]. The most commonly used transparent conductors are wide-gap metal oxides (transparent conducting oxides or TCOs) such as doped indium oxide, zinc oxide, or tin oxide. Transparent conductors need to have low resistivity ($\sim 10^{-4}$ $\Omega\,\mathrm{cm}$) and high transparency (>85%) in the visible and near-ultraviolet spectral range [1,2]. The current TCO market is dominated by indium oxides such as $\mathrm{In_2O_3:Sn}$ (ITO) due to their excellent electrical and optical performance [3,4]. Since indium is a rare element in the Earth's crust, the high demand of ITO in various industries has driven up the price of indium considerably. Hence, there is a great incentive to find replacements for the expensive ITO [3,4]. One of these low-cost alternatives is aluminum-doped zinc oxide (AZO) [5] with electrical and optical properties approaching those of ITO.

Cadmium oxide (CdO) with rocksalt crystal structure (space group = Fm-$3m$) is one of the oldest TCO studied and has received growing attention recently due to its high propensity for *n*-type doping and high electron mobility [6–13]. Previous studies have shown that native defects play a dominant role in electrical and optical properties of CdO. Based on hybrid density functional theory, Burbano *et al.* found that oxygen vacancy constitutes the dominate intrinsic donor defect, while the compensation by acceptor defects would not occur until its Fermi level reaching 1.2 eV above the conduction-band minimum [14]. Yu *et al.* performed thermal annealing studies of sputter-deposited CdO in O_2 and N_2 atmosphere and showed that the high electron concentration in sputter-deposited films can be attributed to O-related native defects [15].

The high quality of CdO thin films can be grown by a variety of deposition methods. For instance, Yan *et al.*

*Corresponding author.
kinmanyu@cityu.edu.hk

reported the epitaxial growth of CdO:Sn film on the MgO (111) substrate by pulsed laser deposition, achieving a conductivity of 4.2×10^4 S/cm and a mobility of 609 $cm^2/V\,s$ at a carrier concentration of 4.74×10^{20} cm^{-3} [6]. Yu *et al.* demonstrated that doped CdO thin film deposited on glass substrates can exhibit high conductivity as well as high transparency in the visible-to-IR spectral range, making it an ideal transparent electrode for high-efficiency multijunction photovoltaic devices [7]. Because of its large static dielectric constant ($\varepsilon_o = 21.9$) [16], CdO has very high electron mobility because of reduced electron scattering through efficient screening of Coulomb potentials of ionized donors. The high electron mobility allows for highly conductive CdO with a relatively low, mid-($10^{20}/cm^3$) electron concentration, and, therefore, low free-carrier absorption that enables high transparency up to the >1200-nm range [7,9,17].

For transparent conductor applications, CdO thin films with >mid-($10^{20}/cm^3$) carrier concentration is needed to achieve a resistivity $< \sim 10^{-4}$ Ω cm. Such a high concentration of free carriers significantly alters optical properties of a semiconductor. For instance, the onset of band-edge absorption in degenerate semiconductor blueshifts due to the large amount of free carriers filling in the conduction band. This effect is known as the Burstein-Moss effect. At the same time, strong free-carrier absorption would be present in the near-infrared (NIR) spectral range [18], and this will narrow the transmission window in the long wavelength regime.

For TCO materials, it is of great importance to understand the effect of free carriers on their optoelectronic properties [19–22]. Optical studies of TCOs are typically carried out using conventional transmittance-reflectance [7,23–25] as well as spectroscopic-ellipsometry (SE) measurements. SE has received increased attention in recent years [26] as a fast, reliable, and highly sensitive method for measuring optical properties of thin film materials. Using polarized light as the probe, SE measures the change in the polarization state of light reflected from (or transmitted through) the surface of a sample over a wide spectral window, providing several unique advantages as compared to the transmittance-reflectance measurement [27]. First, two parameters (Ψ and Δ) instead of one are independently determined in a single measurement at each wavelength. Therefore, both the real and imaginary parts of the complex dielectric function can be obtained directly on a wavelength-by-wavelength basis without having to resort to multiple measurements or to performing the Kramers-Kronig analysis. Second, SE measurement is highly surface sensitive and can be used to measure film down to a submonolayer thickness. The variable angle measurement allows acquiring a large amount of data and minimizing parameter correlations in the model fitting. Finally, SE measures the reflected intensity with reference to the incident light, and hence no special reference sample is needed and results are not affected by fluctuations in the source intensity.

Optical properties of common TCOs such ITO and AZO have been studied by SE [5,19,28]. The effects of free carriers on the optical response of doped TCO thin films were found to be significant, in both the IR and the band-edge region. It has been shown that in Al-doped ZnO thin films with a carrier density of 1×10^{21} cm^{-3} the free-carrier plasma contribution to the dielectric function in the IR region screens the polar-lattice-mode excitation, and results in a Burstein-Moss effect related blueshift of the optical absorption edge [5]. Similar effects should be observed for high carrier concentration, intentionally doped CdO thin films. However, to date only a few SE investigations on CdO have been reported [8]. In this paper, we report a comprehensive study of optical properties of CdO thin films doped with two different types of dopants: shallow donors (In and Ga) and transition metals (V and Ti) with an electron concentration as high as $2 \times 10^{21}/cm^3$ using variable angle spectroscopic ellipsometry (VASE) in the spectral range of 190 to 1700 nm (0.73 to 6.5 eV). Moreover, the electron effective mass for films with different dopants is derived from SE and Hall effect measurements.

II. EXPERIMENT

CdO thin-film samples are deposited using a dual-gun radio-frequency magnetron sputtering system. In, Ga, Ti, and V doping is achieved by using a In_2O_3, Ga_2O_3, TiO_2, and V_2O_3 target, respectively, sputtered together with a CdO target. Some of the In-doped CdO films are also deposited using a 2% and 4% In-doped CdO sintered target. The dopant concentration is tuned by varying the sputtering power and the substrate-target distance of dopant targets. Both soda-lime glass and silicon substrates are used with a substrate temperature maintained at 270 °C during deposition. Prior to deposition, the chamber is pumped down to $\sim 1 \times 10^{-6}$ Torr, and the background pressure is maintained at 5 mTorr by flowing pure Ar or Ar mixed with O_2 (1%–2%) during deposition.

Film stoichiometry, dopant concentration, and thickness are measured by Rutherford backscattering (RBS) using a 3.04 MeV He^{++} beam. Film thicknesses in the range of 100-350 nm are measured by RBS and also confirmed by SE. The crystalline structure of films is determined by x-ray diffraction. Typically, polycrystalline films with a grain size in the range of 10–24 nm are synthesized. Carrier concentration and Hall mobility are obtained from Hall measurement in the van der Pauw configuration. Room temperature SE spectra (the amplitude ratio ψ, and the phase difference Δ) are measured in the spectral range of 0.73 to 6.5 eV using a rotating-compensator instrument (J. A. Woollam, M-2000). The angle of incidence is varied from 60° to 75° with an increment of 5°. The back side of the glass substrate is taped with translucent plastic tape to eliminate back-side

reflection [29]. The rotating compensator ellipsometer provides accurate results for the ellipsometric parameters ψ and Δ over the complete measurement range ($\psi = 0°$–$90°$, $\Delta = 0°$–$360°$). This is a clear advantage over the commonly used rotating-analyzer (polarizer) ellipsometer whose measurement errors increase significantly when Δ approaches 0° and 180° [19,30].

III. SE ANALYSIS

SE data analysis is carried out using a three-layer structure, including a surface roughness layer, CdO film, and glass substrate. The refractive index (n) of the glass substrate is determined by fitting the ellipsometric parameter ψ while the extinction coefficient (k) is obtained by fitting the normal incidence transmission spectrum on a bare glass substrate, according to the procedure outlined in the WVASE32 [31]. The dielectric function of the surface roughness layer is modeled as a 50/50-vol % mixture of the CdO bulk layer and voids [32]. The optical response of free electrons in metal or metal-like materials is typically described by the Drude model [19,31], while for TCO materials, a variety of models including the Lorentz model, the Tauc-Lorentz (TL) model, and the Cauchy model have been used to account for contributions from interband optical transitions. Here, for highly conducting CdO thin films the Drude model combined with the Tauc-Lorentz model is used to describe the dielectric function $\varepsilon(E)$ as

$$\varepsilon(E) = \varepsilon_1(E) - i\varepsilon_2(E) = \varepsilon_D(E) + \varepsilon_{\mathrm{TL}}(E), \tag{1}$$

where $\varepsilon_D(E)$ and $\varepsilon_{\mathrm{TL}}(E)$ are the dielectric functions calculated by the Drude and TL models, respectively. $\varepsilon_D(E)$ describes the intraband, while $\varepsilon_{\mathrm{TL}}(E)$ accounts for the interband optical transitions in the film. This combined model has been used successfully to fit the SE data of SnO_2:F, ZnO:Ga, and In_2O_3:Sn films [19,33,34]. $\varepsilon_D(E)$ is given by

$$\varepsilon_D(E) = -\frac{A_D}{E^2 - i\Gamma_D E}, \tag{2}$$

where the two parameters (A_D, Γ_D) represent the amplitude and the broadening, respectively. Based on the Drude theory, the amplitude A_D can be expressed as

$$A_D = \varepsilon_\infty E_p^2, \tag{3}$$

where ε_∞ and E_p are the high-frequency dielectric constant and plasma energy, respectively. The plasma energy, in turn, can be written as

$$E_p = \hbar\omega_p = \sqrt{\frac{\hbar^2 e^2 N_{\mathrm{opt}}}{m^* \varepsilon_\infty \varepsilon_o}}. \tag{4}$$

In Eq. (4) ω_p, e, N_{opt}, and ε_o are the plasma angular frequency, electron charge, optical carrier concentration, and the free-space permittivity, respectively. The broadening parameter in the Drude model is related with the electron effective mass (m^*) and the optical mobility (μ_{opt}) by

$$\Gamma_D = \frac{\hbar e}{m^* \mu_{\mathrm{opt}}}. \tag{5}$$

At sufficiently low energies, the real part of the dielectric function $\varepsilon_1(E)$ can be written as

$$\varepsilon_1(E) = \varepsilon_\infty - \frac{A_D}{E^2 + \Gamma_D^2}. \tag{6}$$

Hence, ε_∞ can be obtained from the intercept of $\varepsilon_1(E)$ plotted against $1/(E^2 + {\Gamma_D}^2)$ [19,35,36].

In the TL model $\varepsilon_{\mathrm{TL}}(E) = \varepsilon_{\mathrm{TL1}} + i\varepsilon_{\mathrm{TL2}}$, where

$$\varepsilon_{\mathrm{TL2}} = \left[\frac{A_{\mathrm{TL}} E_o C (E - E_T)^2}{(E^2 - E_o^2)^2 + C^2 E^2} \frac{1}{E}\right] \quad \text{for } E > E_T, \tag{7}$$

$$\varepsilon_{\mathrm{TL2}} = 0 \quad \text{for } E < E_T. \tag{8}$$

The $\varepsilon_{\mathrm{TL1}}$ obtained by the Kramers-Kronig relation and integration is given by

$$\varepsilon_{\mathrm{TL1}}(E) = \varepsilon_1(\infty) + \frac{2}{\pi} P \int_{E_T}^{\infty} \frac{\xi \varepsilon_{\mathrm{TL2}}(\xi)}{\xi^2 - E^2} d\xi, \tag{9}$$

with P being the Cauchy principal part of the integral [37]. Thus, in the TL model, the dielectric function is described by five parameters $\{A_{\mathrm{TL}}, E_o, C, E_T, \varepsilon_1(\infty)\}$, which represent the amplitude, center energy, broadening, Tauc optical gap, and energy-independent contribution to the real part of the dielectric function, respectively. Therefore, the various optical and electronic properties such as ε_∞, E_p, N_{opt}, μ_{opt}, and m^* can be derived from the experimentally determined dielectric function.

IV. RESULTS AND DISCUSSION

A. Electrical properties

The electrical properties of CdO films doped with In, Ga, V, and Ti with various doping concentration (given in mole percent) obtained by Hall-effect measurements are summarized in Fig. 1. All the dopant species studied in this work are efficient donors in CdO and, as shown in Fig. 1(a), electron concentration N increases to $>10^{21}/\mathrm{cm}^3$ with a dopant concentration up to 6–10 mole fraction (or 2.3–$3.8 \times 10^{21}/\mathrm{cm}^3$). However, as is seen in Fig. 1(b), there is a significant difference in the electron mobility behavior between group-III shallow donors (Ga and In) and transition metal (V and Ti) dopants. While a high mobility of $\sim$130 $\mathrm{cm}^2/\mathrm{V\,s}$ can be achieved for doping with group-III donors for $n \sim 10^{21}/\mathrm{cm}^3$, doping with transition metals (TMs) results in a rapid drop in the mobility from 90 to

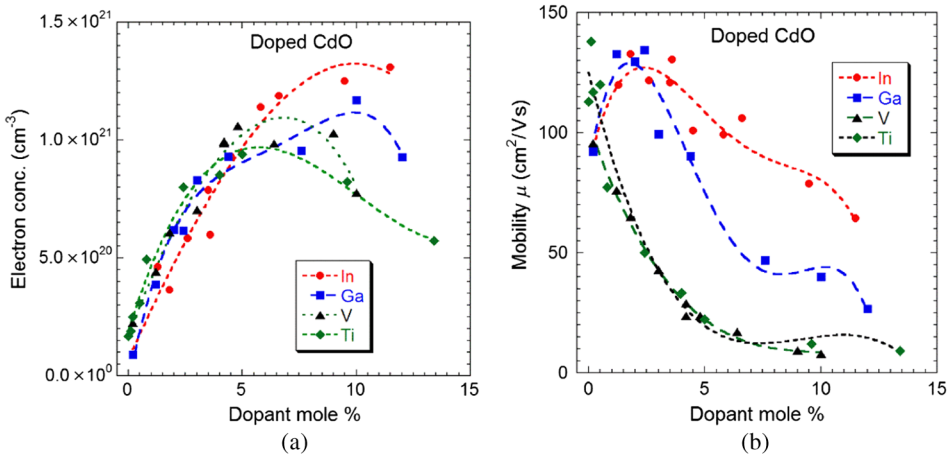

FIG. 1. Electron concentration (a) and mobility (b) for CdO films doped with group III (Ga and In) and transition metal (V and Ti) dopants with increasing dopant concentration. The dashed lines are guides to the eyes using simple polynomial fitting of data points.

<10 cm^2/V s at high electron concentrations. The dramatic difference in the mobility behavior can be attributed to the different doping mechanisms of the two types of dopants. The column-III dopants (Ga and In) substituting Cd sites contribute two electrons to the bonds, and the third loosely bound electron falls into the conduction band and is responsible for the *n*-type conductivity in CdO. On the other hand, group 3*d* TM-substituting Cd contributes two outer 4 s electrons to the bonds, and their electrical activity depends on the location of the donor or acceptor level associated with the 3*d* band. Thus, as has been shown before, the energy of the donor *d* levels of V and Ti are located at ~5.0 and 4.8 eV below the vacuum level, respectively [38], placing these levels at about 1 eV above the CdO conduction-band edge located at ~5.8 eV. Consequently, both V and Ti provide free electrons to the conduction band of CdO until the Fermi level reaches the localized *d*-level energy. The electronic structure parameters derived from an analysis of the spectroscopic-ellipsometry measurements will help us to better understand these different doping mechanisms.

B. Complex dielectric functions

Figure 2 shows the measured (black dotted line) SE spectra of an In-doped CdO (CdO:In) thin film with a Hall electron concentration (N_{Hall}) of 6.6×10^{20} cm^{-3}. We find that, as is shown in Fig. 2, the adopted dielectric function model (solid curve) can fit the experimental SE data very well if the energy range is confined to lower than 3.5 eV. This is understandable, as our simple model cannot be used to describe the optical function at energies much higher than the band gap [19]. Nevertheless, an optical response with a photon energy up to 3.5 eV is sufficient for us to investigate the effects of free carriers in CdO thin films with band-edge absorption at an energy less than 3.5 eV. The corresponding fitting parameters for SE data shown in Fig. 2 are given in Table I.

The complex dielectric function and the complex refractive index of CdO:In thin films with different N_{Hall} are shown in Fig. 3. As seen from the imaginary part of the dielectric function (ε_2) or the extinction coefficient (k), significant free-carrier absorption in the NIR region is observed with high N_{Hall}. The plasma energy (E_p) can be extracted at the photon energy where $\varepsilon_1(E) = 0$. Because of the limited IR energy range for the SE measurement, the E_p could not be obtained for thin films with an electron concentration lower than 5×10^{20} cm^{-3}. As seen in Fig. 3(b), the refractive index (n) increases with the photon energy, with a trend similar to that found in other TCOs [39]. For a CdO thin film with extremely high carrier concentration, the refractive index drops drastically at low energy (e.g., <1 eV or $\lambda > 1200$ nm). Furthermore, as is

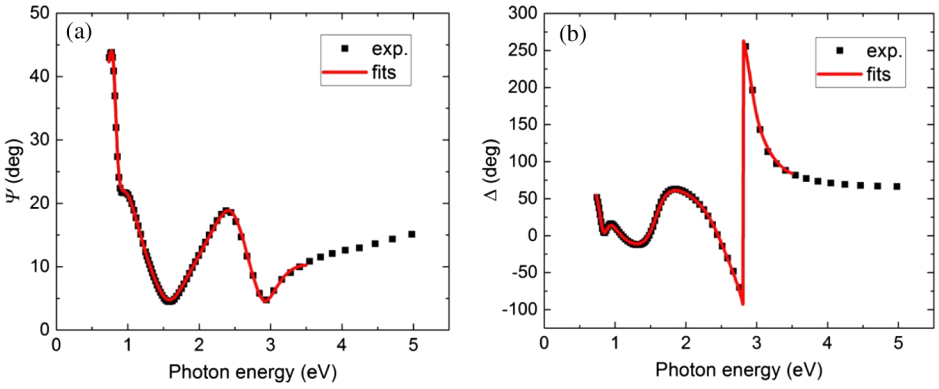

FIG. 2. The measured (black square) and the fitted (red solid line) SE spectra (Ψ and Δ in (a) and (b), respectively) of CdO:In thin film, with $N_{\mathrm{Hall}} = 6.6 \times 10^{20}$ cm^{-3} and angle of incidence of 70°.

TABLE I. The fitting parameters extracted from the dielectric function modeling using the Drude model and Tauc-Lorentz model for CdO:In thin film on glass substrate, with $N_{\mathrm{Hall}} = 6.6 \times 10^{20}$ cm^{-3}. The dopant (In) concentration in the film is around 4%.

CdO:In ($N_{\mathrm{Hall}} = 6.6 \times 10^{20}$ cm^{-3})	
d_s (nm)	5.208 ± 0.084
d_f (nm)	119.22 ± 0.09
A_D	3.0256 ± 0.0040
Γ_D	0.0588 ± 0.0003
A_{TL} (eV)	221.5 ± 16.0
C (eV)	7.751 ± 0.246
E_T (eV)	2.584 ± 0.008
E_0 (eV)	3.990 ± 0.168
ε_1 (∞)	1 (fixed)
MSE	19.4

seen in Fig. 3(b) n of CdO:In films decreases with increasing N_{Hall}, e.g., at a photon energy of 2 eV n decreases from 2.3 to 2 as N_{Hall} increases from 2.3×10^{20} to 1.18×10^{21}/cm^3.

C. Free-carrier absorption and refractive index

In order to get more accurate dielectric functions in a wide spectral range, we fit the SE data by using a more elaborate dielectric function model in which we add two more Gaussian oscillators to the Drude model and combine it with the TL model. The extracted complex dielectric functions of CdO thin films with $N_{\mathrm{Hall}} \sim 8 \times 10^{20}$ cm^{-3} doped with different dopants as well as that of a typical undoped CdO thin film with $N_{\mathrm{Hall}} = 1.2910^{20}$ cm^{-3} are shown in Fig. 4(a). It is worth noting that the obtained dielectric function of undoped CdO thin film is rather close to that of single-crystalline CdO film with a similar carrier concentration ($N_{\mathrm{Hall}} = 210^{20}$ cm^{-3}), as reported by Choi *et al.* [8]. Absorption coefficients of these samples derived from the dielectric functions are shown in Fig. 4(b). As expected, the absorption edge of the doped CdO sample with high N_{Hall} blueshifts due to the Burstein-Moss effect. At the same time, free-carrier absorption α_{FCA} becomes significant in the low energy region $0.74 < E < 1$ eV for the films with high carrier concentration. It is interesting to note that as is shown in the inset of Fig. 4(b), the low photon-energy absorption coefficient α is dependent on the dopant species. Thus, with similar N_{Hall} of $\sim 8 \times 10^{20}$ cm^{-3}, α is larger in the TM-doped films than In- or Ga-doped films for $E > 0.9$ eV and smaller for $E < 0.8$ eV.

Based on the Drude model, α_{FCA} are given by $Ne^2/[\varepsilon_o cn\mu(m^*\omega)^2]$, with N being the free-carrier concentration, e the electron charge, ε_o the permittivity in free space, c the speed of light in vacuum, n the refractive index of material, μ the carrier mobility, m^* the electron effective mass, and ω the photon angular frequency [18]. The dotted lines in the inset of Fig. 4(b) are calculated using the effective mass and the optical mobility derived from Eqs. (4) and (5) (discussed in the following sections) for the doped samples, while for the undoped thin film, $m^* = 0.23m_e$ and $\mu = 84$ cm^2/V s (Hall mobility) are assumed. The calculated α_{FCA} agree well with α at relatively low energy, indicating that α_{FCA} dominates the absorption at low energies. Since $\alpha_{\mathrm{FCA}} \propto N/\mu$, the higher α_{FCA} of TM-doped CdO thin films at $E > 0.8$ eV is mainly attributed to their lower carrier mobility; while the lower α_{FCA} at energy $E < 0.8$ eV for the TM-doped CdO is due to their much larger refractive index (e.g., $n \sim 0.7$ for CdO:V and $n \sim 0.13$ for CdO:In).

The dependence of free-carrier absorption in the NIR region at a wavelength of 1200 nm and the refractive index (n) in the visible region at 600 nm on the N_{Hall} are shown in Figs. 5(a) and 5(b), respectively. Figure 5(a) shows that for all dopants $\alpha(\lambda = 1200\ \mathrm{nm})$ generally increases with N_{Hall} and then tends to saturate at a high electron concentration for all dopants. Specifically, α increases from 10^2 cm^{-1} to 1×10^4 cm^{-1} as N_{Hall} increases from 2×10^{20} cm^{-3} to 12×10^{20} cm^{-3}. We note that for $N_{\mathrm{Hall}} > 5 \times 10^{20}$/cm^3 doping with In or Ga results in over 2 to 3 times lower absorption compared with the samples doped with TMs. As mentioned earlier, this difference in α is attributed to the low mobility of TM-doped materials [7].

As is seen in Fig. 5(b), the refractive index of doped CdO thin film taken at $\lambda = 600$ nm is monotonously decreasing

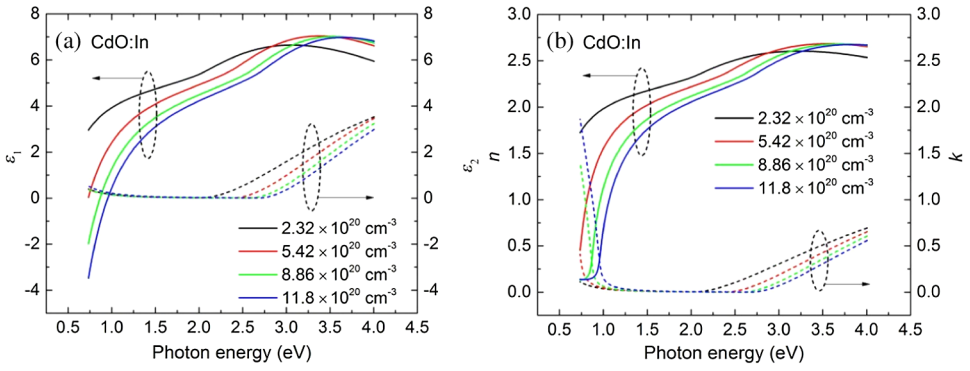

FIG. 3. The complex dielectric function (a) and the complex refractive index (b) extracted from the optical model for CdO:In thin films with variable N_{Hall}.

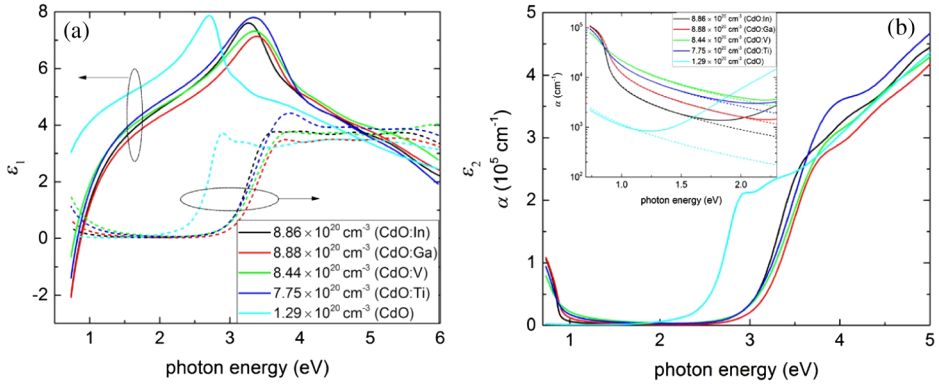

FIG. 4. The complex dielectric function of doped (In, Ga, V, Ti) CdO thin film with similar N_{Hall} (a), and the absorption coefficient of the doped CdO thin films (b). The inset in (b) is the corresponding α in a smaller energy range (0.74–2.3 eV) in the log scale, with the dotted lines representing the calculated α_{FCA}. The undoped CdO thin film with $N_{\mathrm{Hall}} \approx 1.29 \times 10^{20}$ cm^{-3} is also shown for comparison.

with increasing N_{Hall}. Unlike the absorption coefficient, the refractive index $n(\lambda = 600\ \mathrm{nm})$ does not show any discernible dependence on the different dopant species. Carrier-induced change in the refractive index is related to the change in absorption coefficient $\Delta\alpha$, given by

$$\Delta n(E) = \frac{2c\hbar}{e^2} P \int_0^\infty \frac{\Delta\alpha(E')}{E'^2 - E^2}\, dE', \tag{10}$$

where c is the speed of light, e is the electron charge, E is the photon energy, and P indicates the principal value of the integral [40]. The free-carrier-induced change of the absorption coefficient $\Delta\alpha$ is caused by three diffident effects: Burstein-Moss shift, band-gap renormalization, and the free-carrier absorption effect. In the Drude model, the intraband free-carrier absorption induced change in the refractive index is given by $\Delta n = -(e^2\lambda^2 N/8\pi^2 c^2 \varepsilon_0 n m^*)$, where the N is the electron concentration [40]. The linear decrease in $n(\lambda = 600\ \mathrm{nm})$ of doped CdO thin film most likely related to the fact that both free-carrier absorption and the Burstein-Moss effect induced change in the refractive index linearly depend on the free-carrier concentration [40]. Note that the refractive index of doped or undoped CdO thin film with low-carrier concentration $N_{\mathrm{Hall}} < 3 \times 10^{20}$ cm^{-3} is equal to ~2.3 at 600 nm. This is close to the value reported for epitaxial CdO film with N_{Hall} of 2×10^{20} cm^{-3} [8]. The refractive index of TCO is an important parameter in optical design for optoelectronic devices, e.g., in a solar-cell device where the TCO serves as the front electrode, and could be as an antireflection coating [41]. For instance, for the silicon solar cell with $n \sim 3.9$ at 600 nm the minimum light reflection is achieved for TCO with $n = 2.4$, which is very close to that of CdO thin films.

D. High-frequency dielectric constant

Figure 6(a) shows plots of ε_2 of CdO:In thin films with different N_{Hall} as a function of $1/(E^2 + \Gamma_D^2)$. As indicated in Eq. (6), the high-frequency dielectric constant ε_∞ can be obtained from the x intercept of these plots. Values of ε_∞ for CdO doped with different dopants (In, Ga, V, Ti) are plotted as a function of N_{Hall} in Fig. 6(b). We observe that the ε_∞ of CdO decreases roughly linearly from ~5.5 to 4.9 with increasing N_{Hall} with no obvious dependence of the dopant species. Such linear dependence of ε_∞ on carrier concentration was also found for other TCOs, e.g., ZnO:Ga (GZO) and In_2O_3:Sn [19]. The ε_∞ values of CdO thin films with different carrier concentration obtained from SE measurements are close to that reported by Finkenrath *et al.* [42] and are much higher than those of other conventional TCOs. For CdO, ITO, and GZO with electron concentration $N = 10^{21}/\mathrm{cm}^3$, the respective values of ε_∞ are 5.0, 4.05, and 3.6 for [19].

The values of plasma wavelength λ_p obtained from Eq. (4) for doped CdO thin films are shown in Fig. 7. The λ_p of In or Ga-doped CdO thin film with variable

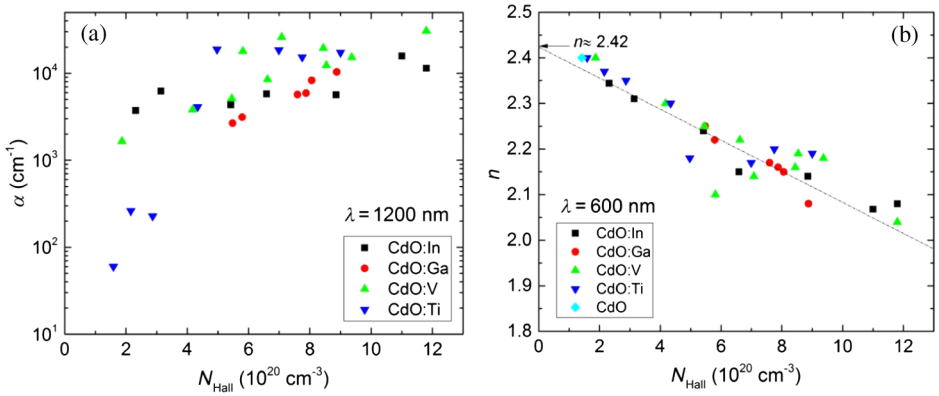

FIG. 5. Absorption coefficient (a) at a wavelength of 1200 nm and the refractive index (b) at a wavelength of 600 nm of CdO thin films doped with various dopants (In, Ga, V, Ti) obtained from SE analysis. The refractive index of undoped CdO thin film is also given for reference.

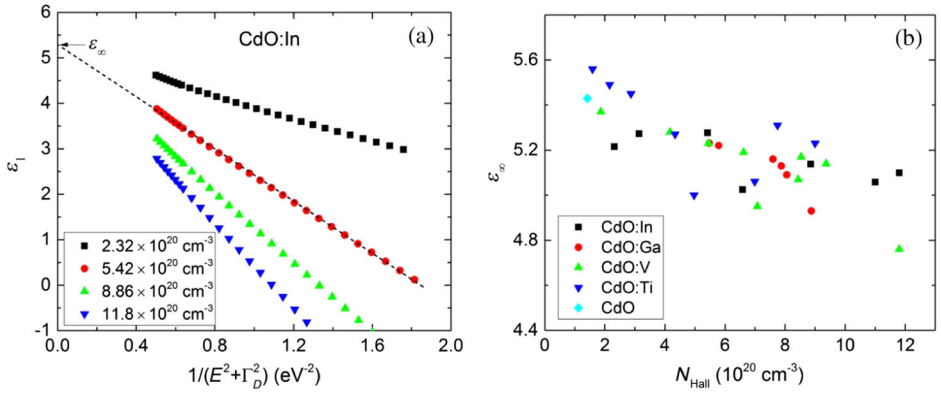

FIG. 6. The real part of dielectric function ε_1 (a) plotted as function of $1/(E^2+\Gamma_D^2)$, and the high-frequency dielectric constant (b) of CdO thin films with dependence on Hall carrier concentration.

carrier concentration is consistent with our previous work, in which the λ_p is obtained by fitting the experimental reflectance spectrum using a constant effective mass of $0.2m_o$ [7]. In contrast, λ_p of TM-doped CdO films are much larger. This can be attributed to the enhancement of the electron effective mass by TM doping (see Eq. 4). As is seen in Fig. 7, λ_p values for ITO, AZO, and GZO adopted from the literature are consistently smaller than that of CdO. The higher λ_p for CdO broadens the transparency window and makes this material particularly suited for transparent conductor applications in the IR regime.

E. Electron effective mass

Using the values of ε_∞ shown in Fig. 6(b) and assuming $N_{\rm opt} = N_{\rm Hall}$ one can calculate the electron effective mass m^* of CdO from Eq. (4). The results in Fig. 8 show that the effective mass nonlinearly increases with $N_{\rm Hall}$. In addition, a rapid increase of the effective mass is observed in TM-doped CdO at $N_{\rm Hall} > 8\times10^{20}$ cm^{-3}. The dependence of m^* on electron concentration in In- and Ga-doped samples can be explained by a nonparabolicity of the conduction band of CdO in a way similar to that used for other TCOs [44,45]

$$m^* = m_o^*\sqrt{1+2C\frac{\hbar^2}{m_o^*}(3\pi^2N)^{2/3}}, \tag{11}$$

where m_o^* is the effective mass at the bottom of the conduction band, C is a nonparabolicity parameter, N is the carrier concentration and is taken as $N_{\rm Hall}$ here. The black solid line shown in Fig. 8 is the best fit of the effective mass data for the In- and Ga-doped CdO samples with m_0^* and C as fitting parameters. The best-fit results for m_o^* and C are $0.13\pm0.04m_o$ and 0.5 ± 0.2 eV^{-1}, respectively. Here, m_o is the free electron mass. Fits with m_o^* fixed at 0.1 and $0.2m_o$ (dash lines) are also shown for comparison. In our previous work [7], a higher band-edge effective mass $m_o^* = 0.2m_o$ was assumed. However, Fig. 8 shows that a reasonable fit of our data cannot be obtained by assuming a $m_o^* = 0.2m_o$. Note that m_o^* ranging from 0.12 to 0.2 has been reported [17,46–48]. Unlike most reports where

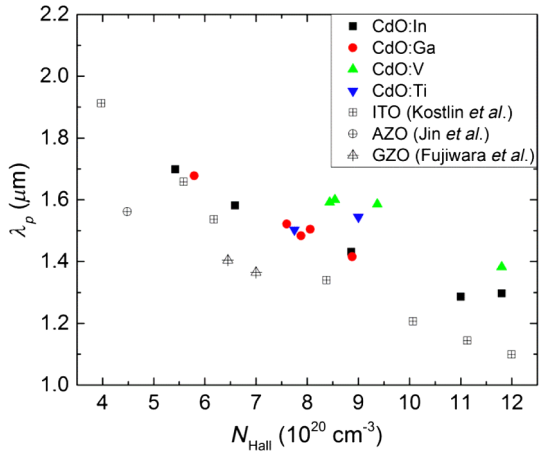

FIG. 7. The plasma wavelength obtained from SE analysis for doped CdO thin films as a function of $N_{\rm Hall}$. The previously reported results for other TCOs by Kostlin *et al.* (Ref. [43]), Jin *et al.* (Ref. [24]), and Fujiwara *et al.* (Ref. [19]) are also shown for comparison.

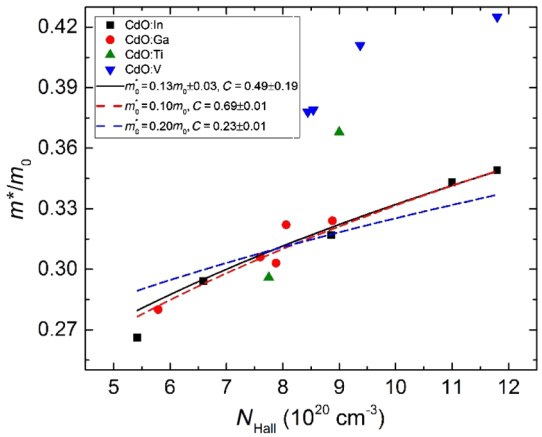

FIG. 8. Electron effective mass $m*$ for CdO thin films with different dopants as a function of $N_{\rm Hall}$, where m_o is the free electron mass. The black line is the best fit for data from the In- and Ga-doped samples by using Eq. (11); the dashed lines are fits with fixed m_0^* with values of 0.1 and $0.2m_o$.

TABLE II. A comparison of parameters of CdO obtained from SE measurements and those for ITO and GZO/AZO from the literature.

	CdO (this work)	ITO	GZO/AZO
n ($\lambda = 600$ nm) ($N = 7 \times 10^{20}/\mathrm{cm}^3$)	2.2	1.8 [19,49] ~1.9 [50]	1.7 ([19], GZO)
ε_∞ ($N = 0$)	5.4	4.62 [19]	3.9 ([19], GZO)
ε_∞ ($N = 1 \times 10^{21}/\mathrm{cm}^3$)	5.0	4.05 [17], ~3.0 [50] <3.0 [49]	3.6 ([19], GZO)
C (eV^{-1})	0.5	0.18 [19], 0.5 [28]	0.142 ([19], GZO)
m_o^*/m_o	0.13	0.3 [19] 0.18 [28]	0.28 ([19], GZO) 0.30 ([51], GZO)
m^* ($N = 1 \times 10^{21}/\mathrm{cm}^3$)	0.33	0.407 [19] 0.4 [28], ~0.38 [50]	0.38 ([19], GZO) 0.43 ([52], AZO)

the effective mass is obtained by assuming a constant high-frequency dielectric constant ε_∞, the m^* in Fig. 8 are calculated using the carrier-concentration-dependent ε_∞ in Fig. 6(b). The nonparabolicity parameter C of CdO obtained in this work is very close to that reported for ITO ($C \sim 0.5\ \mathrm{eV}^{-1}$) by Feneberg *et al.* [28], but much higher than that of GZO ($C \sim 0.142\ \mathrm{eV}^{-1}$) reported by Fujiwara *et al.* [19]. Table II shows a comparison of various parameters of In and Ga-doped CdO with the literature values of these parameters for ITO and GZO.

The much-higher effective mass obtained for the TM-doped CdO is related to the presence of partially occupied d states of the dopant species. Garcia-Hemme *et al.* have shown by optical absorption and photoluminescence measurements that the anticrossing interaction between the localized d levels of V atoms and the extended states of the ZnO CB results in an upward shift of the mostly unoccupied conduction-band states (E_+ subband) and broadening of the occupied V donor d levels into a narrow band (E_- subband) [53]. Such anticrossing interaction also occurs in the TM-doped CdO resulting in a modification of the conduction-band dispersion relation. The flattening of the dispersion relation for the E_- subband is reflected in an increase in the electron effective mass.

F. Optical band gap

The absorption coefficient (α) can be calculated from the measured extinction coefficient k using the equation $\alpha = 4\pi k/\lambda$. Assuming the transition probability becomes constant at the absorption edge, the absorption coefficient for the direct allowed transition can be estimated as $\alpha \approx (E - E_G^{\mathrm{Opt}})^{1/2}$ [54]. The optical band gap E_G^{opt} can then be estimated by extrapolating α^2 to zero photon energy. Figure 9(a) shows $\alpha^2(E)$ plots for CdO:In films with different N_{Hall} and the E_G^{opt} obtained are plotted in Fig. 9(b). Since highly conducting TCOs are typically degenerately doped, the optical band gap E_G^{opt} is larger than its intrinsic band gap due to the Burstein-Moss effect and band-gap renormalization [55,56].

The optical band gap of a heavily doped n-type semiconductor can be expressed as

$$E_G^{\mathrm{opt}} = E_G + \Delta E_G^{\mathrm{BM}} - \Delta E^{\mathrm{BGN}}, \tag{12}$$

where E_G, ΔE_G^{BM}, ΔE^{BGN} are the intrinsic band gap, the Burstein-Moss shift, and the band-gap renormalization, respectively [55–57]. In this work, the ΔE_G^{BM} is calculated by using the nonparabolic conduction-band model [44], while the band-gap renormalization is evaluated by Jain's model [58,59],

$$\frac{\Delta E^{\mathrm{BGN}}}{R} = \frac{1.83}{r_s}\frac{\Lambda}{N_b^{1/3}} + \frac{0.95}{r_s^{3/4}} + \frac{\pi}{2}\frac{1}{r_s^{3/4}N_b}\left(1 + \frac{m_{\mathrm{min}}^*}{m_{\mathrm{maj}}^*}\right), \tag{13}$$

where R is the effective Rydberg energy, N_b is the number of equivalent band extrema, Λ is the correction factor accounting for anisotropy of bands in n-type semiconductors and interaction between the heavy-and light-hole bands

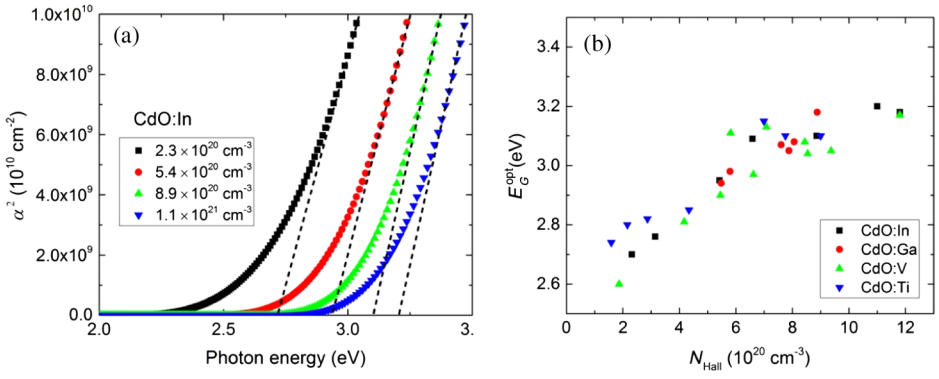

FIG. 9. Plotting of α^2 as a function of photon energy for CdO:In films with different N_{Hall} (a), and optical band gap of doped CdO thin films as a function of N_{Hall} (b).

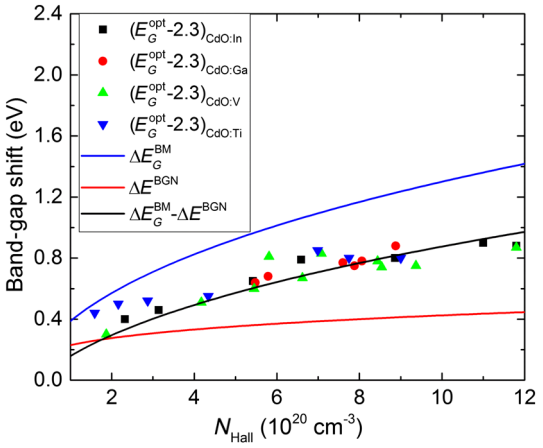

FIG. 10. Band-gap shift of doped CdO thin films as a function of N_{Hall}, assuming an intrinsic band gap of 2.3 eV. The calculated Burstein-Moss shift ΔE_G^{BM}, the band-gap renormalization ΔE^{BGN}, as well as $\Delta E_G^{\mathrm{BM}} - \Delta E^{\mathrm{BGN}}$ are also illustrated.

in p-type semiconductors, r_s is the average distance (normalized to the effective Bohr radius) between majority carriers, and m^*_{min} and m^*_{maj} are minority and majority carrier density of state effective masses, respectively. The parameter values used for calculating ΔE^{BGN} by Eq. (13) are adopted from work by Zhu *et al.* [57]. Figure 10 shows the band-gap shift $(E_G^{\mathrm{opt}} - E_G)$ for doped CdO thin films as a function of N_{Hall}. Here, the intrinsic band gap E_G of 2.3 eV for CdO is used. The calculated ΔE_G^{BM}, ΔE^{BGN}, and $\Delta E_G^{\mathrm{BM}} - \Delta E^{\mathrm{BGN}}$ are also shown for comparison. We find that band-gap shift $(E_G^{\mathrm{opt}} - E_G)$ for the doped CdO thin films agrees well with the calculated values, and the apparent shifts are independent of the dopant species.

G. Optical mobility

The optical mobility μ_{opt} is determined from the experimentally measured broadening parameter Γ_D using Eq. (5). Figure 11(a) compares μ_{opt} of doped CdO films with the mobility measured by the Hall effect μ_{Hall}. The effective mass shown in Fig. 8 is used in the calculation. The dotted line in Fig. 11(a) indicates the case when $\mu_{\mathrm{opt}} = \mu_{\mathrm{Hall}}$. As shown in Fig. 11(a), μ_{opt} is very close to μ_{Hall} when $\mu_{\mathrm{Hall}} < 60$ cm^2/V s. However, for doped CdO films with $\mu_{\mathrm{Hall}} > 60$ cm^2/V s, we find that $\mu_{\mathrm{opt}} < \mu_{\mathrm{Hall}}$. It has been argued that the μ_{opt} represents an average intragrain mobility of polycrystalline materials and is generally higher than μ_{Hall} since μ_{Hall} represents the average mobility of electrons undergoing multiple-grain-boundary scattering [17]. $\mu_{\mathrm{Hall}} \geq \mu_{\mathrm{opt}}$ suggests that the mobility of CdO is not affected by grain-boundary scattering. This is consistent with the high electron affinity (5.8 eV) of CdO, which gives rise to electron accumulation at CdO grain boundaries.

Based on the degenerate electron gas model, the mean free path of electrons is given by

$$L_e = (3\pi^2)^{1/3}\left(\frac{\hbar}{e^2}\right)\rho^{-1}N^{-2/3}, \tag{14}$$

where ρ and the N are the resistivity and the carrier concentration, respectively [60,61]. The average grain size (D) of CdO films estimated from x-ray diffraction measurements is ~10–25 nm. Figure 11(b) shows a plot of D/L_e as a function of μ_{Hall} for the In- and Ga-doped CdO. We find that for films with high mobility, which have $\mu_{\mathrm{Hall}} \geq \mu_{\mathrm{opt}}$, the grain size is comparable to or smaller than the electron mean free path ($D/L_e \leq 1$). This again suggests that the effect of grain-boundary scattering on the μ_{Hall} is negligible in these films.

Although cases with $\mu_{\mathrm{opt}} < \mu_{\mathrm{Hall}}$ were also previously reported for In_2O_3:Sn [19], SnO_2:F [62], and CdO:In films grown by cathodic arc deposition [17], there is no clear explanation on this phenomenon. Mendelsberg *et al.* suggested that electrons crossing the grain boundaries during the optical excitation may bring μ_{opt} closer to μ_{Hall} for films with small grains and large electron mean free path (L_e) [17]. It should be noted that the Hall effect measures electron transport laterally across the film, while SE probes the film in the vertical direction. It is possible that electron transport is not isotropic in these films.

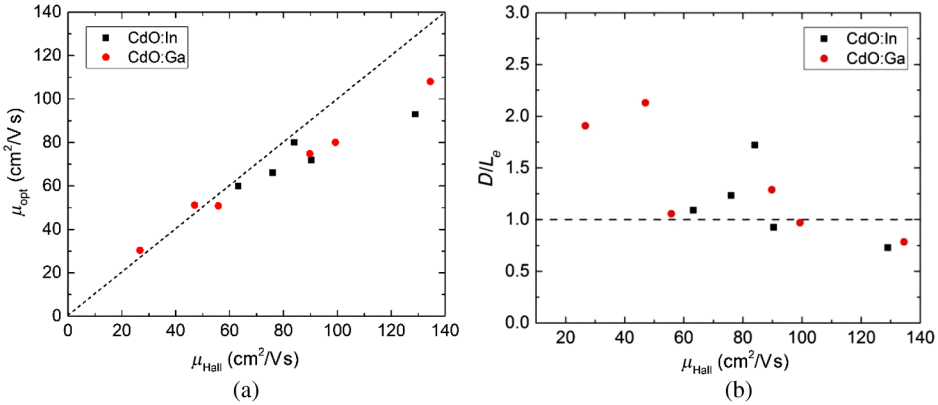

FIG. 11 (a) Optical mobility (μ_{opt}) obtained from SE analysis using the effective mass presented in Fig. 8, and (b) mean free path of CdO thin films as a function of μ_{Hall}.

V. CONCLUSIONS

We study the effects of the free electrons on electro-optical properties of CdO thin films doped with different dopants (In, Ga, V, Ti). Samples with carrier concentration ranging from 2×10^{20} cm^{-3} to 12×10^{20} cm^{-3} are measured using spectroscopic ellipsometry. It is found that free carriers significantly affect the complex dielectric function of doped CdO thin films. Analysis of SE data using a combined Drude and Tauc-Lorentz model provides various material parameters, including refractive index $n(\lambda)$, high-frequency dielectric constant ε_∞, electron mass m^*, plasma wavelength λ_p, free-carrier absorption, optical band gap E_G^{opt}, and optical mobility μ_{opt}. We observe that with increasing carrier concentration, (i) ε_∞ decreases roughly linearly from ~5.6 to 4.8, (ii) α in the NIR region increases significantly due to free-carrier absorption, (iii) the E_G^{opt} increases due to Burstein-Moss and band-gap renormalization effects from 2.3 to 3.2 eV, (iv) λ_p decreases, and (v) the m^* for In- and Ga-doped CdO increases from $0.13m_o$ for electrons at the bottom of the conduction band to $0.33m_o$. The dependence of m^* on the carrier concentration is consistent with the prediction from the nonparabolic conduction-band model. For transition-metal-doped CdO, at high doping ($N > 8 \times 10^{20}/\text{cm}^3$) the m^* deviates significantly from the nonparabolic model and is ~20%–30% higher than that for Ga and In-doped materials. This is attributed to the modification of the CdO CB by the interaction of localized d states of the TM dopants with the extended CdO CB state. Our measured results of doped CdO thin films with high mobility, low resistivity, long plasma reflection wavelength, low free electron absorption, large high-frequency dielectric constant, and high refractive index make them an ideal transparent conductor, especially when transmission of IR photons ($\lambda > 1000$ nm) is required.

ACKNOWLEDGMENTS

This work was supported by the City University of Hong Kong (Project No. 9380076). Material synthesis and RBS analysis performed at LBNL were supported by the Electronic Materials Program at the Lawrence Berkeley National Laboratory. J. A. Z. acknowledges support by the Research Grants Council, University Grants Committee, Hong Kong (Project No. CityU 122812). Y. F. was supported by the Hong Kong Ph.D. Fellowship No. PF-15139, Research Grants Council, University Grants Committee, Hong Kong.

[1] D. S. Ginley, H. Hosono, and D. C. Paine, *Handbook of Transparent Conductor* (Springer, New York, 2010).

[2] K. Ellmer, Past achievements and future challenges in the development of optically transparent electrodes, Nat. Photonics **6**, 809 (2012).

[3] C. I. Bright, *50 Years of Vacuum Coating Technology and the Growth of the Society of Vacuum Coaters* (Society of Vacuum Coaters, Ohio, 2007), Chap. VII.

[4] T. Minami, Present status of transparent conducting oxide thin-film development for indium-tin-oxide (ITO) substitutes, Thin Solid Films **516**, 5822 (2008).

[5] *Transparent Conductive Zinc Oxide: Basics and Applications in Thin Film Solar Cells*, edited by K. Ellmer, A. Klein, and B. Rech (Springer, New York, 2008).

[6] M. Yan, M. Lane, C. R. Kannewurf, and R. P. H. Chang, Highly conductive epitaxial CdO thin films prepared by pulsed laser deposition, Appl. Phys. Lett. **78**, 2342 (2001).

[7] K. M. Yu, M. A. Mayer, D. T. Speaks, H. He, R. Zhao, L. Hsu, S. S. Mao, E. E. Haller, and W. Walukiewicz, Ideal transparent conductors for full spectrum photovoltaics, J. Appl. Phys. **111**, 123505 (2012).

[8] S. G. Choi, J. Z. Perez, V. M. Sanjose, A. G. Norman, C. L. Perkins, and D. H. Levi, Complex dielectric function and refractive index spectra of epitaxial CdO thin film grown on *r*-plane sapphire from 0.74 to 6.45 eV, J. Vac. Sci. Technol. B **28**, 1120 (2010).

[9] C. E. Ekuma, J. Moreno, and M. Jarell, Electronic, transport, optical and structural properties of rocksalt CdO, J. Appl. Phys. **114**, 153705 (2013).

[10] S. K. V. Farahani, T. D. Veal, P. D. C. King, J. Z. Perez, V. M. Sanjose, and C. F. McConville, Electron mobility in CdO films, J. Appl. Phys. **109**, 073712 (2011).

[11] S. Jin, Y. Yang, J. E. Medvedeva, L. Wang, S. Li, N. Cortes, J. R. Ireland, A. W. Metz, J. Ni, M. C. Hersam, A. J. Freeman, and T. J. Marks, Tuning the properties of transparent oxide conductors dopant ion size and electronic structure effects on CdO-based transparent conducting oxide Ga- and In-doped CdO thin film grown by MOCVD, Chem. Mater. **20**, 220 (2008).

[12] J. J. Mudd, T. L. Lee, V. M. Sanjose, J. Zuniga Perez, D. Hesp, J. M. Kahk, D. J. Payne, R. G. Egdell, and C. F. McConville, Hard x-ray photoelectron spectroscopy as a probe of the intrinsic electronic properties of CdO, Phys. Rev. B **89**, 035203 (2014).

[13] I. N. Demchenko, M. Chernyshova, T. Tyliszczak, J. D. Denlinger, K. M. Yu, D. T. Speaks, O. Hemmers, W. Walukiewicz, G. Derkachov, and K. L. Jablonska, Electronic structure of CdO studied by soft x-ray spectroscopy, J. Electron Spectrosc. Relat. Phenom. **184**, 249 (2011).

[14] M. Burbano, D. O. Scanlon, and G. W. Watson, Source of conductivity and doping limits in CdO from hybrid density functional theory, J. Am. Chem. Soc. **133**, 15065 (2011).

[15] Kin Man Yu, D. M. Detert, Guibin Chen, Wei Zhu, Chaoping Liu, S. Grankowska, O. D. Dubon, Leon Hsu, and Wladek Walukiewicz, Defects, and properties of cadmium oxide based transparent conductors, J. Appl. Phys. **119**, 181501 (2016).

[16] H. Finkenrath and N. Uhie, Der einfluss der gitterschwingungen auf die ultrarot-reflexion von CdO, Solid State Commun. **5**, 875 (1967).

[17] R. J. Mendelsberg, Y. Zhu, and A. Anders, Determining the nonparabolicity factor of the CdO conduction band using indium doping and the Drude theory, J. Phys. D **45**, 425302 (2012).

[18] M. Fox, *Optical Properties of Solids* (Oxford University Press, New York, 2010).

[19] H. Fujiwara and M. Kondo, Effects of carrier concentration on the dielectric function of ZnO : Ga and In_2O_3 : Sn studied by spectroscopy ellipsometry: Analysis of free-carrier and band-edge absorption, Phys. Rev. B **71**, 075109 (2005).

[20] J. A. Stoke, J. D. Beach, W. C. Bradford, and T. R. Ohno, Electrical and optical properties of magnetron sputtered Cd_2SnO_4 transparent conducting oxide thin films for use in CdTe solar devices, Thin Solid Films **562**, 254 (2014).

[21] P. P. Edwards, A. Porch, M. O. Jones, D. V. Morgan, and R. M. Perks, Basic materials physics of transparent conducting oxides, Dalton Trans. 2995 (2004).

[22] T. Yamada, H. Makino, N. Yamamoto, and T. Yamamoto, Ingrain and grain boundary scattering effects on electron mobility of transparent conducting polycrystalline Ga-doped ZnO films, J. Appl. Phys. **107**, 123534 (2010).

[23] I. Hamberg and C. G. Granqvist, Evaporated Sn-doped In_2O_3 films: Basic optical properties and applications to energy efficient windows, J. Appl. Phys. **60**, R123 (1986).

[24] Z. C. Jin, I. Hamberg, and C. G. Granqvist, Optical properties of sputter-deposited ZnO:Al thin films, J. Appl. Phys. **64**, 5117 (1988).

[25] Y. Qu, T. A. Gessert, K. Ramanathan, R. G. Dhere, R. Noufi, and T. J. Coutts, Electrical and optical properties of ion beam sputtered ZnO:Al as a function of film thickness, J. Vac. Sci. Technol. A **11**, 996 (1993).

[26] D. E. Aspnes, Spectroscopic ellipsometry—Past, present, and future, Thin Solid Films **571**, 334 (2014).

[27] *Handbook of Ellipsometry*, edited by H. G. Tompkins and E. A. Irene (Springer-Verlag, Berlin, 2005).

[28] M. Feneberg, J. Nixdorf, C. Lidig, R. Goldhahn, Z. Galazka, O. Bierwagen, and J. S. Speck, Many-electron effects on the dielectric function of cubic In_2O_3: Effective electron mass, band nonparabolicity, band gap renormalization, and Burstein-Moss shift, Phys. Rev. B **93**, 045203 (2016).

[29] R. A. Synowicki, Suppression of backside reflections from transparent substrates, Phys. Status Solidi C **5**, 1085 (2008).

[30] J. Lee, P. I. Rovira, I. An, and R. W. Collins, Rotating-compensator multichannel ellipsometry: Applications for real time Stokes vector spectroscopy of thin film growth, Rev. Sci. Instrum. **69**, 1800 (1998).

[31] J. A. Woollam, *Guide to Using WVASE32®* (J. A. Woollam Co., Inc., Lincoln, 2008).

[32] D. E. Aspnes, Optical properties of thin films, Thin Solid Films **89**, 249 (1982).

[33] P. I. Rovira and R. W. Collins, Analysis of specular and textured SnO_2:F by high speed four-parameter Stokes vectors spectroscopy, J. Appl. Phys. **85**, 2015 (1999).

[34] T. Yamada, H. Makino, N. Yamamoto, and T. Yamanoto, Ingrain and grain boundary scattering effects on electron mobility of transparent conducting polycrystalline Ga-doped ZnO films, J. Appl. Phys. **107**, 123534 (2010).

[35] E. Shanthi, V. Dutta, A. Banerjee, and K. L. Chopra, Electrical and optical properties of undoped and antimony-doped tin oxide films, J. Appl. Phys. **51**, 6243 (1980).

[36] E. Shanthi, A. Banerjee, V. Dutta, and K. L. Chopra, J. Appl. Phys. **53**, 1615 (1982).

[37] G. E. Jellison Jr. and F. A. Modine, Parameterization of the optical functions of amorphous materials in the interband region, Appl. Phys. Lett. **69**, 371 (1996); Appl. Phys. Lett. **69**, 2137(E) (1996).

[38] J. M. Langer, C. Delerue, M. Lannoo, and H. Heinrich, Transition-metal impurities in semiconductors and heterojunction band lineups, Phys. Rev. B **38**, 7723 (1988).

[39] F. Ruske, in *Physics and Technology of Amorphous-Crystalline Heterostructure Silicon Solar Cells*, edited by W. G. J. H. M. van Sark, L. Korte, and F. Roca (Springer Berlin Heidelberg, 2012).

[40] B. R. Bennett, R. A. Soref, and J. A. Del Alamo, Carrier-induced change in refractive index of InP, GaAs, and InGaAsP, IEEE J. Quantum Electron. **26**, 113 (1990).

[41] *Thin Film Solar Cells: Fabrication, Characterization and Applications,* edited by J. Poortmans and V. Arkhipov (John Wiley & Sons, Ltd, Chichester, 2006).

[42] H. Finkenrath, H. Kohler, and M. Lochmann, Optische eigenabsorption und dielektrizitatskonstantevon kadmiumoxyd bei hoher elektronenentartung, Z. Angew. Phys. **21**, 512 (1966).

[43] H. Kostlin, R. Jost, and W. Lems, Optical and electrical properties of doped In_2O_3 films, Phys. Status Solidi A **29**, 87 (1975).

[44] T. Pisarkiewicz, K. Zakrzewska, and E. Leja, Scattering of charge carriers in transparent and conducting thin oxide films with a non-parabolic conduction band, Thin Solid Films **174**, 217 (1989).

[45] T. Pisarkiewicz and A. Kolodziej, Nonparabolicity of the conduction band structure in degenerate tin dioxide, Phys. Status Solidi B **K5**, 158 (1990).

[46] Y. Dou, T. Fishlock, R. G. Egdell, D. S. L. Law, and G. Beamson, Band-gap shrinkage in n-type-doped CdO probed by photoemission spectroscopy, Phys. Rev. B **55**, R13381 (1997).

[47] T. J. Coutts, D. L. Young, X. Li, W. P. Mulligan, and X. Wu, Search for improved transparent conducting oxides: A fundamental investigation of CdO, Cd_2, SnO_4, and Zn_2SnO_4, J. Vac. Sci. Technol. A **18**, 2646 (2000).

[48] P. H. Jefferson, S. A. Hatfield, T. D. Veal, P. D. C. King, C. F. McConville, J. Z. Perez, and V. M. Sanjose, Bandgap and effective mass of epitaxial cadmium oxide, Appl. Phys. Lett. **92**, 022101 (2008).

[49] J. A. Woollam, W. A. McGahan, and B. Johs, Spectroscopic ellipsometry studies of indium tin oxide and other flat panel display multilayer materials, Thin Solid Films **241**, 44 (1994).

[50] T. Nagatomo, Y. Maruta, and O. Omoto, Electrical and optical properties of vacuum evaporated indium-tin oxide films with high electron mobility, Thin Solid Films, **192**, 17 (1990).

[51] N. Preissler, O. Bierwagen, A. T. Ramu, and J. S. Speck, Electrical transport, electrothermal transport, and effective electron mass in single-crystalline In_2O_3 films, Phys. Rev. B **88**, 085305 (2013).

[52] A. V. Singh, R. M. Mehra, A. Yoshida, and A. Wakahara, Doping mechanism in aluminum doped zinc oxide films, J. Appl. Phys. **95**, 3640 (2004).

[53] E. García-Hemme, K. M. Yu, P. Wahnon, G. González-Díaz, and W. Walukievicz, Effects of *d*-donor level of vanadium on the properties of $Zn_{1-x}V_xO$ films, Appl. Phys. Lett. **106**, 182101 (2015).

[54] Y. Ohhata, F. Shinoki, and S. Yoshida, Optical properties of R.F. reactive sputtered tin-doped In_2O_3 films, Thin Solid Films **59**, 255 (1979).

[55] I. Hamberg, C. G. Granqvist, K. F. Berggren, B. E. Sernelius, and L. Engstrom, Band-gap widening in heavily Sn-doped In_2O_3, Phys. Rev. B **30**, 3240 (1984).

[56] B. E. Sernelius, K. F. Berggren, Z. C. Jin, I. Hamberg, and C. G. Granqvist, Band-gap tailoring of ZnO by means of heavy Al doping, Phys. Rev. B **37**, 10244 (1988).

[57] Y. Zhu, R. J. Mendelsberg, J. Zhu, J. Han, and A. Anders, Structural, optical and electrical properties of indium-doped cadmium oxide films prepared by pulsed filtered cathodic arc deposition, J. Mater. Sci. **48**, 3789 (2013).

[58] S. C. Jain, J. M. McGregor, and D. J. Roulston, Band-gap narrowing in novel III-V semiconductors, J. Appl. Phys. **68**, 3747 (1990)

[59] S. C. Jain and D. J. Roulston, A simple expression for band gap narrowing (BGN) in heavily doped Si, Ge, GaAs and Ge_xSi_{1-x} strained layers, Solid-State Electronics **34**, 453 (1991).

[60] C. Kittel, *Introduction to Solid State Physics,* 7th ed. (Wiley, New York, 1996).

[61] T. Yamanoto, T. Sakemi, K. Awai, and S. Shirakata, Dependence of carrier concentrations on oxygen pressure for Ga-doped ZnO prepared by ion plating method, Thin Solid Films **451**, 439 (2004).

[62] M. Akagawa and H. Fujiwara, Optical characterization of textured SnO_2:F layers using spectroscopic ellipsometry, J. Appl. Phys. **112**, 083507 (2012).